Int. Conference on Boundary and Interior Layers
BAIL 2006
G. Lube, G. Rapin (Eds)

Rarefied Gas Boundary Layer Predicted with Continuum and Kinetic Approaches

Koji Morinishi

Department of Mechanical and System Engineering
Kyoto Institute of Technology
Matsugasaki, Sakyo-ku, Kyoto 606-8585, Japan
morinisi@kit.ac.jp

1. Introduction

Numerical simulation of low speed gas flows about micro devices is one of the recent new frontiers of computational fluid dynamics (CFD). It may provides essential understanding about the fluid behavior around micro-electro-mechanical systems (MEMS). Since the flows about the micro devices just range from slip to transitional flow regimes, numerical methods based on the Boltzmann equation or the Navier-Stokes equations subject to velocity slip and temperature jump boundary conditions must be used.

One of the well-known numerical methods for the Boltzmann equation is the direct simulation Monte Carlo (DSMC) method [1]. The DSMC method has been widely used for simulating high speed rarefied flows [2]. The method, however, becomes a poor simulation tool for the low speed flows about micro devices, because huge sample size is required to reduce its inherent statistical scatter to a level of the small changes of flow quantities in the low speed flows [3]. A deterministic CFD method [4, 5] based on a kinetic model Boltzmann equation is free from the statistical scatter and is definitely superior to the DSMC method for the low speed flows. While these kinetic methods can be applied theoretically to any flow regimes from continuum to free molecule, application to the continuum or slip flow regimes is prohibitively expensive in the computational cost, and application to the transitional flow regime is most preferable.

The Navier-Stokes methods may be able to predict flows in the slip regime, if the velocity slip and temperature jump boundary conditions are introduced. Although theoretical applicability of the Navier-Stokes methods to the transitional flow regime is negative, the application is preferable in the computational cost because the Navier-Stokes methods are computationally several orders of magnitude more inexpensive than the Boltzmann methods. Thus it is fairly meaningful to compare the prediction of the Navier-Stokes methods with that of the Boltzmann methods in order to verify the applicability and limitation of the Navier-Stokes methods.

2. Kinetic approach

The motion of gas molecules at any Knudsen number is governed by the well known Boltzmann equation. Because of its complex collision integral term, however, the solution of the Boltzmann equation requires an exceedingly formidable task except for few simple problems. In this paper, instead of the full Boltzmann equation, a kinetic model equation [6] is used, which correctly resembles the lower 13 moments (the density, three components of the velocity, six components of the stress tensor, and three components of the heat flux) of the Boltzmann equations. The kinetic model Boltzmann equation in nondimensional form without any external force may be written as follows:

$$\frac{\partial f}{\partial t} + \mathbf{c} \cdot \frac{\partial f}{\partial \mathbf{x}} = \nu(f_0 - f) \tag{1}$$

where f is the velocity distribution function which depends on the time t, the physical space $\mathbf{x}$, and the molecular velocity $\mathbf{c}$. The distribution function f_0 of the BGK model [7], which is the most fundamental model, is the local equilibrium distribution function f_e:

$$f_e = \frac{n}{(\pi T)^{3/2}} \exp\left(-\frac{(\mathbf{c}-\mathbf{u})^2}{T}\right) \tag{2}$$

where n is the number density, $\mathbf{u}$ the macroscopic flow velocity, and T the temperature. For a higher order model equation which correctly resembles the lower 13 moments of the Boltzmann equation [6], the distribution function f_0 is given as

$$f_0 = f_e\left[1 + 2(1-Pr)\frac{(\mathbf{c}-\mathbf{u})\cdot\mathbf{q}}{5pT}\left(\frac{2(\mathbf{c}-\mathbf{u})^2}{T} - 5\right)\right] \tag{3}$$

where p is the pressure, $\mathbf{q}$ the heat flux vector, and Pr the Prandtl number (=2/3 for a monatomic gas).

The macroscopic flow quantities are obtained from the distribution function as

$$\begin{aligned} n &= \int f d\mathbf{c} \\ n\mathbf{u} &= \int \mathbf{c} f d\mathbf{c} \\ \frac{3}{2}nT &= \int (\mathbf{c}-\mathbf{u})^2 f d\mathbf{c} \\ \mathbf{q} &= \int (\mathbf{c}-\mathbf{u})(\mathbf{c}-\mathbf{u})^2 f d\mathbf{c} \end{aligned} \tag{4}$$

For numerical quadrature, simple equally spaced trapezoidal rule is used in this study. The pressure p is obtained from the equation of state:

$$p = nT \tag{5}$$

All these quantities are normalized with a reference length L, a reference number density n_∞, a reference temperature T_∞, and a reference velocity C_∞. The reference velocity C_∞ is the most probable molecular thermal speed which is defined as:

$$C_\infty = \sqrt{2RT_\infty} \tag{6}$$

The collision frequency ν is usually defined as:

$$\nu = \frac{8nT^{1-s}}{5\sqrt{\pi}Kn} \tag{7}$$

where Kn is the reference Knudsen number based on the reference length L and the molecular mean free path λ_∞ at reference state which is defined as

$$\lambda_\infty = \frac{16\mu_\infty}{5mn_\infty\sqrt{2\pi RT_\infty}} \tag{8}$$

where μ is the viscosity coefficient, m the mass of a molecule, and R the gas constant. The viscosity coefficient is assumed to depend on the temperature as:

$$\mu \propto T^s \tag{9}$$

where the Maxwell molecules correspond to the power s of 1 and the hard sphere molecules to 0.5. In this study, the hard sphere molecules is adopted.

An upwind gridless method [8] is adopted for estimation of the convective terms of the equation. Gradients of any function f at a computational point i may be evaluated with the following linear combination form in the cloud of neighboring points $C(i)$.

$$\nabla f = \sum_{k \subset C(i)} \mathbf{a}_{ik} f_{ik} \tag{10}$$

where the subscript k denotes the index of the point which belongs to the cloud $C(i)$. The sum is obtained over all member points of $C(i)$ except the point i itself. The function values f_{ik} are evaluated at the midpoint between the points i and k.

The coefficients $\mathbf{a}_{ik}$ are once obtained at the beginning of computation and stored if the points remain stationary. Several methods can be used for obtaining the coefficients [8]. If the approximation (10) is applied in a finite volume cell, the coefficients may be obtained from the unit normal and area of the cell surface, and the cell volume.

The convective terms of the kinetic model equations (1) for two dimensional flows can be evaluated with the gridless method, for an example, as:

$$\left(c_x \frac{\partial f}{\partial x} + c_y \frac{\partial f}{\partial y} \right) \Bigg|_i = \sum_{k \subset C(i)} \xi_{ik} f_{ik} \tag{11}$$

where ξ_{ik} is defined as:

$$\xi_{ik} = a_{xik} c_x + a_{yik} c_y \tag{12}$$

The numerical flux $\xi_{ik} f_{ik}$ are estimated as

$$\xi_{ik} f_{ik} = \frac{1}{2} \left\{ \xi_{ik} (f_{ik}^+ + f_{ik}^-) - |\xi_{ik}| (f_{ik}^+ - f_{ik}^-) \right\} \tag{13}$$

The third order accurate weighted essentially non-oscillatory (WENO) method [9] is used for reconstructing the midpoint distribution function $f_{ik}^{\pm}$ [10].

After evaluating the convective and collision terms, following implicit Euler method is used for the temporal discretization of the kinetic model equation.

$$\left(\frac{1}{\Delta t_i} + \nu + \sum_{k \subset C(i)} \xi_{ik}^+ \right) \Delta f_i + \sum_{k \subset C(i)} \xi_{ik}^- \Delta f_k = RHS_i \tag{14}$$

where RHS are the evaluation of the convective and collision terms and $\xi^{\pm}$ are defined as follows

$$\xi^{\pm} = \frac{1}{2} (\xi \pm |\xi|) \tag{15}$$

The solution of this linear system of equation (14) can be obtained with a lower-upper symmetric Gauss-Seidel (LU-SGS) procedure [11] as:

$$\Delta f_i^* = D_i^{-1} \left(RHS_i - \sum_{k \subset L(i)} \xi_{ik}^- \Delta f_k \right) \tag{16}$$

$$\Delta f_i = \Delta f_i^* - D_i^{-1} \sum_{k \subset U(i)} \xi_{ik}^- \Delta f_k \tag{17}$$

where $C(i) = L(i) \bigcup U(i)$ and D_i are defined with

$$D_i = \left(\frac{1}{\Delta t_i} + \nu + \frac{1}{2} \sum_{k \subset C(i)} |\xi_{ik}| \right) \tag{18}$$

The distribution function at the next time step g^{n+1} is obtained as:

$$f_i^{n+1} = f_i^n + \Delta f_i \tag{19}$$

where the superscript n denotes the time index.

Perfect diffuse reflection is assumed for the interaction between molecules and solid walls. That is, molecules which strike the solid surface are subsequently emitted with fully accommodating to the wall temperature T_w and velocity $\mathbf{u}_w$.

At inlet and outlet boundaries, the local equilibrium distribution functions are specified for incoming molecules. For outgoing molecules, simple extrapolation of the distribution function is used, which may not affect numerical results because the distribution functions on inner computational points are updated with the upwind gridless solver.

3. Continuum approach

The basic equations of continuum approach is the compressible Navier-Stokes equations which may be written in the following nondimensional form.

$$\frac{\partial \mathbf{Q}}{\partial t} + \nabla \cdot \mathbf{F} = \frac{1}{Re} \nabla \cdot \mathbf{R} \tag{20}$$

where $\mathbf{Q}$ is the conservative vector, $\mathbf{F}$ the convective flux, $\mathbf{R}$ the viscous flux, and Re the reference Reynolds number. The conservative vector and the flux terms are given with:

$$\mathbf{Q} = \begin{pmatrix} \rho \\ \mathbf{u} \\ e \end{pmatrix} \quad , \quad \mathbf{F} = \begin{pmatrix} \rho\mathbf{u} \\ \rho\mathbf{u}\mathbf{u} + p\mathbf{I} \\ \mathbf{u}(e+p) \end{pmatrix} \quad , \quad \mathbf{R} = \begin{pmatrix} 0 \\ \tau \\ \mathbf{u} \cdot \tau - \mathbf{q} \end{pmatrix} \tag{21}$$

where e is the total energy per unit volume, which is given for a perfect gas as:

$$e = \frac{p}{\gamma - 1} + \frac{1}{2}\rho \mathbf{u}^2 \tag{22}$$

Here γ is the ratio of specific heats. The viscous stress tensor τ and the heat flux vector $\mathbf{q}$ are defined with:

$$\tau_{ij} = \mu \left(\frac{\partial u_i}{\partial x_j} + \frac{\partial u_j}{\partial x_i} - \frac{2}{3}\delta_{ij} \frac{\partial u_i}{\partial x_j} \right) \tag{23}$$

$$q_i = -\frac{\gamma}{\gamma - 1} \frac{\mu}{Pr} \frac{\partial T}{\partial x_i} \tag{24}$$

All these quantities in the continuum approach are normalized with a reference length L, a reference density ρ_∞ $(= mn_\infty)$, a reference temperature T_∞, and a reference velocity U_∞. The reference velocity U_∞ is defined as:

$$U_\infty = \sqrt{RT_\infty} \tag{25}$$

where nondimensional velocities in the continuum approach are greater than those in the kinetic approach by the ratio of $\sqrt{2}$.

The Navier-Stokes equations are also solved using the upwind gridless and LU-SGS methods [8]. The convective terms are evaluated with:

$$\begin{aligned} \nabla \cdot \mathbf{F}|_i &= \sum_{k \subset C(i)} (\mathbf{a}_{ik} \cdot \mathbf{F}_{ik}) \\ &= \sum_{k \subset C(i)} \mathbf{G}_{ik} \end{aligned} \tag{26}$$

The flux term $\mathbf{G}$ at the midpoint between the point i and point j is expressed for two dimensional flows as:

$$\mathbf{G} = \begin{pmatrix} \rho U \\ \rho u U + a_x p \\ \rho v U + a_y p \\ U(e+p) \end{pmatrix} \tag{27}$$

where U is defined by

$$U = a_x u + a_y v \tag{28}$$

The numerical flux G_{ik} are estimated as:

$$\mathbf{G}_{ik} = \frac{1}{2}\left\{\mathbf{G}(\tilde{\mathbf{Q}}^+_{ik}) + \mathbf{G}(\tilde{\mathbf{Q}}^-_{ik}) - |\tilde{\mathbf{A}}_{ik}|(\tilde{\mathbf{Q}}^+_{ik} - \tilde{\mathbf{Q}}^-_{ik})\right\} \tag{29}$$

where $\tilde{Q}$ are the primitive variables and $\tilde{A}$ are the flux Jacobian matrices. The primitive variables $\tilde{\mathbf{Q}}^{\pm}_{ik}$ at the midpoint are reconstructed with the third order accurate WENO method [10].

The viscous terms of the Navier-Stokes equations are also evaluated with the gridless method, for an example, as:

$$\frac{\partial}{\partial x}\left(\mu\frac{\partial u}{\partial x}\right)\bigg|_i = \sum_{k\subset C(i)} a_{xik}\left(\mu\frac{\partial u}{\partial x}\right)_{ik} \tag{30}$$

While a simple arithmetical average is used for obtaining μ_{ik}, the first derivatives at the midpoint is evaluated with the following method.

$$\left.\frac{\partial u}{\partial x}\right|_{ik} = \frac{\Delta x}{\Delta s^2}(u_k - u_i) + \frac{1}{2}\frac{\Delta y}{\Delta s^2}\left[\Delta y\left(\left.\frac{\partial u}{\partial x}\right|_i + \left.\frac{\partial u}{\partial x}\right|_k\right) - \Delta x\left(\left.\frac{\partial u}{\partial y}\right|_i + \left.\frac{\partial u}{\partial y}\right|_k\right)\right] \tag{31}$$

Here $\Delta x = x_k - x_i$, $\Delta y = y_k - y_i$, and $\Delta s^2 = \Delta x^2 + \Delta y^2$.

After evaluating the convective and viscous terms, a linearized implicit Euler method is constructed for the temporal discretization of the Navier-Stokes. The solution of this linear system of equations is obtained with the LU-SGS procedure [8].

At the wall surface, the first order slip conditions are implemented as:

$$u_s - u_w = \frac{2-\sigma_v}{\sigma_v} Kn \frac{\mu}{\rho\sqrt{T_w}}\frac{\partial u}{\partial n} + \frac{3}{4}\sqrt{\frac{\pi}{2}} Kn \frac{\mu}{\rho T_w}\frac{\partial T}{\partial s} \tag{32}$$

$$T_s - T_w = \frac{2-\sigma_t}{\sigma_t}\frac{2\gamma}{\gamma+1}\frac{Kn}{Pr}\frac{\mu}{\rho\sqrt{T_w}}\frac{\partial T}{\partial n} \tag{33}$$

where n and s denote the normal and tangential directions to the surface, respectively. The momentum accommodation coefficient σ_v and the energy accommodation coefficient σ_t are set to unity in all the computation presented here.

For inlet and outlet boundaries, characteristic boundary conditions are implemented.

4. Numerical results

In order to verify the applicability and limitation of the Navier-Stokes solver with velocity slip and temperature jump boundary conditions, numerical results obtained with the Navier-Stokes solver are compared with those of the Boltzmann methods. Plane Couette flows and supersonic flows over a circular cylinder are selected as the test problems.

Couette flow is a well defined benchmark problem to validate a numerical method. In this study, upper and lower parallel plates move in the opposite direction each other with the velocity U_∞ and $-U_\infty$, respectively. The reference length is the distance between the two plates. Figures 1 and 2 show the comparison of the velocity profile near the lower plate and temperature profile obtained at a Knudsen number of 0.01 and a Mach number, based on the plate speed, of 0.4.

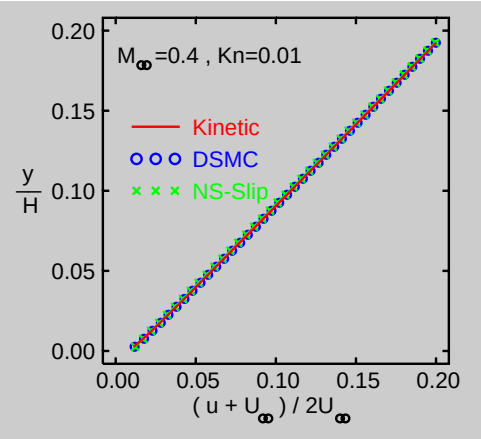

Figure 1: Comparison of velocity profiles for a Couette flow at $M_\infty = 0.4$ and $Kn = 0.01$.

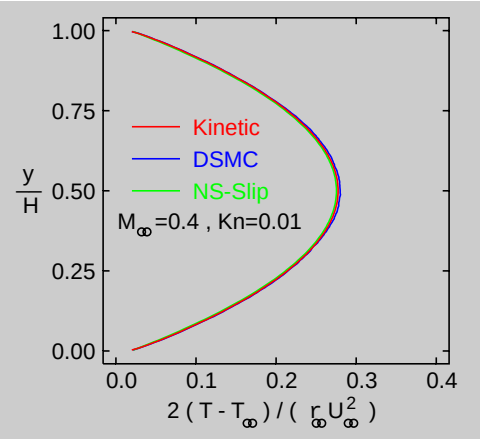

Figure 2: Comparison of temperature profiles for a Coutte flow at $M_\infty = 0.4$ and $Kn = 0.01$.

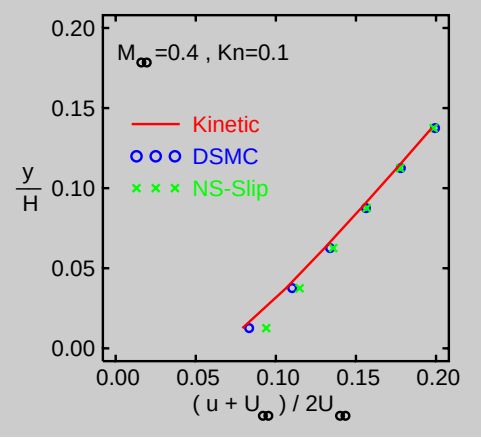

Figure 3: Comparison of velocity profiles for a Couette flow at $M_\infty = 0.4$ and $Kn = 0.1$.

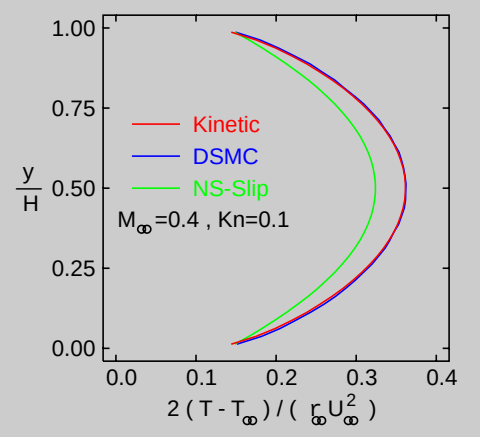

Figure 4: Comparison of temperature profiles for a Coutte flow at $M_\infty = 0.4$ and $Kn = 0.1$.

For this low Knudsen number case, the Navier-Stoke solver with the slip boundary conditions predicts good results compared to those predicted with the kinetic model Boltzmann solver and the DSMC method.

Similar comparison is made at a Knudsen number of 0.1 in Figs. 3 and 4. The Mach number based on the plate speed is unchanged at 0.4. The Navier-Stokes solver well predicts the velocity profile in bulk flow region, while the prediction deviates from the kinetic prediction in the Knudsen layer. The Navier-Stokes solver also fails to predict the temperature profile for this case.

Next a supersonic flow about a circular cylinder at a free stream Mach number of 2.0 and a Knudsen number of 0.1 is simulated. The Knudsen number is estimated based on the diameter of the circular cylinder and the reference mean free path at the free stream. Figures 5 and 6 show the comparison of the density contours and temperature contours, respectively. While the computations are carried out for the whole two dimensional domain with 128×64 cells, the results of the kinetic model Boltzmann solver are plotted for the upper half domain and the slip Navier-Stokes results for the lower half domain. Very good agreement between the kinetic model results and the slip Navier-Stokes results is generally observed in the front region including the position of bow shock. In the wake region, some discrepancy is observed, where the density is

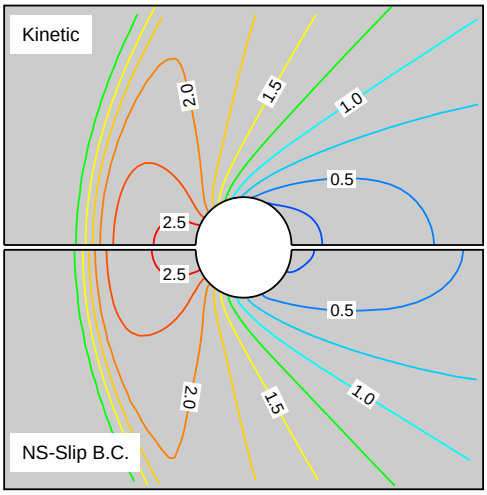

Figure 5: Density contours obtained with kinetic model Boltzmann solver and slip NS solver at $M_\infty = 2.0$ and $Kn = 0.1$.

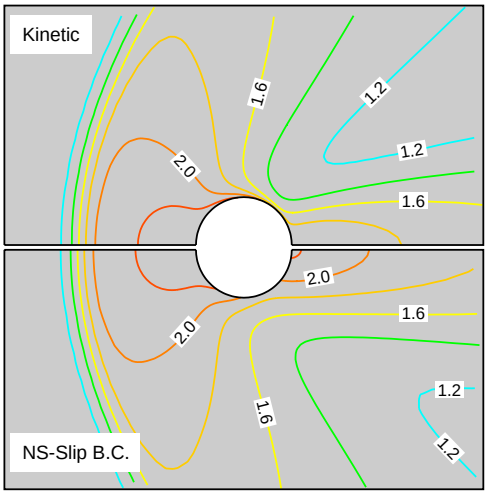

Figure 6: Temperature contours obtained with kinetic model Boltzmann solver and slip NS solver at $M_\infty = 2.0$ and $Kn = 0.1$.

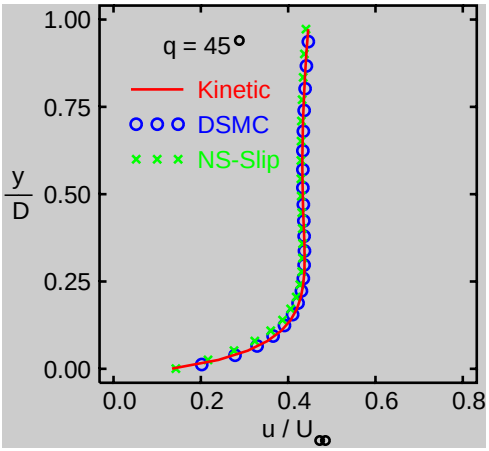

Figure 7: Comparison of tangential velocity profiles at $\theta = \pi/4$.

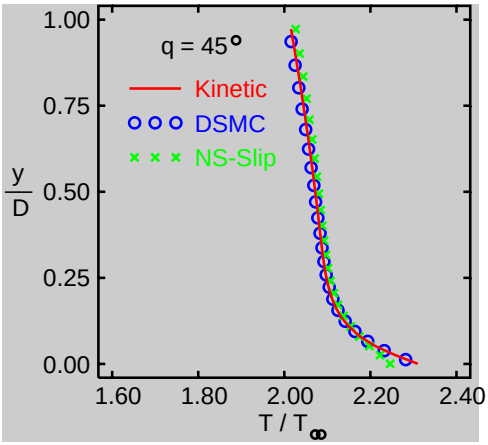

Figure 8: Comparison of temperature profiles at $\theta = \pi/4$.

lower than the free stream density and the rarefactive effect may be pronounced.

Figures 4. to 4. show the comparison of tangential velocity profiles and temperature profiles along the normal lines from the cylinder surface at $\theta = \pi/4$ and $\theta = \pi/2$. The Navier-Stokes prediction is in good agreement with the kinetic predictions at $\theta = \pi/4$, while some discrepancy is observed at $\theta = \pi/2$.

5. Conclusions

Velocity and temperature profiles predicted with a Navier-Stokes solver at slip and transitional flow regimes were compared with those of a kinetic model Boltzmann solver and the DSMC method. For slip flow regime, the Navier-Stokes solver produces the flow field fairly well compared to the Boltzmann solver, while some discrepancy is observed for transitional flow regime.

This study was partly supported by a Grant-in-Aid for Scientific Research (17360079) from the Japan Society for the Promotion of Science.

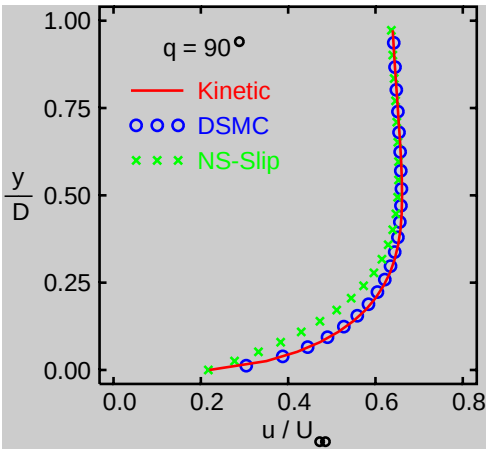

Figure 9: Comparison of tangential velocity profiles at $\theta = \pi/2$.

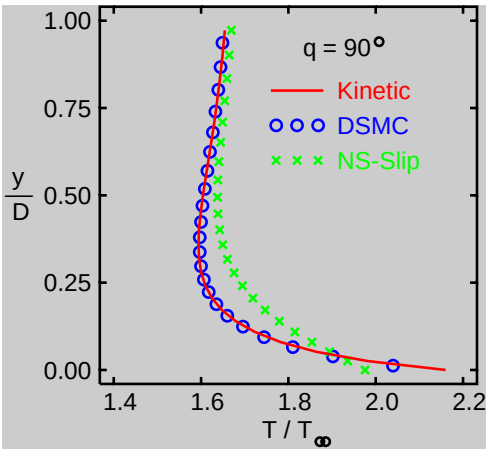

Figure 10: Comparison of temperature profiles at $\theta = \pi/2$.

References

[1] G.A. Bird, *Molecular gas dynamics and the direct simulation of gas flows*, Oxford Science Publications, (1994).

[2] E.S. Oran, C.K. Oh, and B.Z. Cybyk, "Direct simulation Monte Carlo: Recent advances and applications", *Annual Review of Fluid Mechanics*, **30**, 403–442, (1998).

[3] J. Fan, I.D. Boyd, C.P. Cai, "Computation of rarefied gas flows around a NACA0012 airfoil", *AIAA Journal*, **39**, 618–625, (2001).

[4] K. Morinishi and H. Oguchi, "A Computational method and its application to analyses of rarefied gas flows", *Proc. 14th International Symposium on Rarefied Gas Dynamics*, University of Tokyo Press, Vol. 1, 149–158, (1984).

[5] K. Morinishi, "Numerical simulation for gas microflows using Boltzmann equation", *Computers & Fluids*, **35**, 978–985, (2006).

[6] T. Abe and H. Oguchi, "A hierarchy kinetic model and its applications", *Proc. 10th International Symposium on Rarefied Gas Dynamics*, Progress in Astronautics and Aeronautics, AIAA, **58** 781–793, (1977).

[7] P.L. Bhatnager, E.P. Gross, and M. Krook, "A model collision processes in gases. I. Small amplitude processes in charged and neutral one-component system", *Physical Review*, **94**, 511–525, (1954).

[8] K. Morinishi, "A Gridless type solver - Generalized finite difference method -", *Computational Fluid Dynamics for the 21st Century*, Notes on Numerical Fluid Mechanics, Springer, **78**, 43–58, (2001).

[9] G.S. Jiang and C.W. Shu, "Efficient implementation of weighted ENO schemes", *Journal of Computational Physics*, **126**, 202–228, (1996).

[10] K. Morinishi, "Parallel computation of higher order gridless type solver", *Parallel Computational Fluid Dynamics*, Elsevier, 427–434, (2003).

[11] A. Jameson and S. Yoon, "Lower-upper implicit schemes with multiple grids for the Euler equations", *AIAA Journal*, **25**, 929–935, (1987).